
Turbulent Phenomena in the Aerobreakup of Liquid Droplets

Jozsef Nagy^c, Andras Horvath, Christian Jordan and Michael Harasek

Institute of Chemical Engineering, Vienna University of Technology, AUSTRIA

Received: 13/12/2011 – Revised 15/07/2012 – Accepted 05/08/2012

Abstract

This work presents the computational simulation results of turbulent phenomena in a high velocity multiphase flow, where the predominantly turbulent phase is the gaseous phase. For reliable simulation results the code is validated by comparing results of a single phase supersonic turbulent flow to other simulation and experimental results and good agreement is found. This is a precondition for the simulation of the initial stages of the breakup of a liquid droplet in a high Weber number flow. The role of the subgrid-scale turbulence is investigated and two distinct regions are identified. In the second region turbulence phenomena seem to be the predominant factors for the characteristic shape. Simulation results are compared to experiments of the droplet breakup at high Weber number.

Keywords: Aerobreakup; Muktiphase; OpenFOAM[®]; Supersonic; Turbulence.

1. Introduction

The simulation of the turbulent interaction of a high velocity gaseous phase with a liquid phase is a very challenging task. One of the most important applications of such an analysis is the description of the aerobreakup of a liquid droplet. When droplets are exposed to a gaseous high velocity flow (e.g. in a shock tube), they show certain characteristics which have been extensively studied by experiments [1-6]. Simulations of such a process have been done in the past [6-13], however most of the used CFD codes either assume a laminar flow or a DNS approach claiming to reach the Kolmogorov scales of the flow with the calculation grid used. However, very little is known about the turbulent phenomena in the breakup of a liquid droplet. In this paper some insight is given into the turbulent phenomena in such a flow.

For that one has to guarantee that the depiction of the flow field of the high velocity gaseous phase is handled correctly. The simulation of shock waves in a turbulent flow is a widely studied area in aerodynamics. Experimental studies have been conducted [14-15] and in the last decade, as the computational capabilities increased, the simulation of these flows has been intensified [16-19]. The ordinary Reynolds-averaged Navier-Stokes methods struggle to handle the investigated phenomena [16-17] correctly (e.g. expansion-compression corner), however Large Eddy Simulation (LES) and Direct Numerical Simulation (DNS) approaches have been used successfully.

^c Corresponding Author: J. Nagy

Email: jnagy@mail.tuwien.ac.at Telephone: +43-1-58801-166223

© 2009-2012 All rights reserved. ISSR Journals

Fax: +43-1-58801-15999

PII: S2180-1363(12)43112-X

At first, the correct depiction of all the important parts of a single phase high velocity turbulent flow is ensured by using the experiences of past studies. This will be shown in a short investigation of an exemplary single phase case that has been studied both experimentally [14-15] and numerically [16-18].

Once correct results in the gaseous phase are achieved, the interaction of the gaseous and the liquid phase can be analyzed. The main issue of the simulative approach is the high amount of calculation time required due to the large number of cells in the grid. For that reason two-dimensional simulations have been carried out approximating a droplet by an infinitely long cylinder [6-13]. Qualitative extrapolations to the actual three-dimensional droplet case can be assumed, however not all the conclusions can be transferred to the three-dimensional case. Most importantly, turbulence is a three-dimensional phenomenon and a two-dimensional simulation approach often leads to non-physical results. Such differences can be seen by a detailed comparison of two-dimensional simulation results and experimental results. Throughout this work three-dimensional simulations are conducted in order to avoid those problems.

In recent years laser-induced fluorescence has been utilized to visualize liquid droplets that are suddenly exposed to supersonic gas streams [1,6]. Significant differences have been found in comparison to the predecessor approach of the shadowgraph-method. These results show that the simulations do describe the macroscopic shape of the droplet during its deformation. However, there is a need to increase the understanding of the phenomena of smaller scales on the liquid surface. When liquid droplets are suddenly exposed to high speed gas flows, they shatter. At high velocities (i.e. high Weber numbers, large ratios of inertia to surface tension forces) this has been stated in [1] to occur due to the phenomenon of shear-induced entrainment. In [1] a mirror-smooth, central area and an outwardly directed flow were clearly identified. Simulations struggle to depict this sudden change of the shape of the surface of the droplet and the underlying phenomena.

One can find both experimental and simulative investigations of the problem, however, the process as a whole is still under intensive investigation. For one, most of the simulations simplify the flow domain to a two-dimensional problem [8,9,10,13] thus solving the process for an infinitely long cylinder. This assumption is valid to some degree, however, if one wants to understand more detailed parts of the whole process, a three-dimensional approach is needed in order to depict the investigated phenomena in detail. Also most of the simulations do not mention an explicit modeling of turbulence thus implicitly either claiming the negligibility of subgrid-scale turbulent phenomena or assuming the direct numerical simulation (DNS) of turbulence. In this work the authors want to show the effect of three-dimensional explicit turbulence modeling in the aerobreakup of a liquid droplet and its effects onto the shape of the droplet during the initial stages of the breakup process.

The study of additional explicit turbulence modeling of such flows might give an insight into the cause of this sudden change. Therefore in this work the results of three-dimensional simulations with turbulence modeling are summarized. For the simulations the open source CFD library OpenFOAM® (version 1.7.1) [20-22] was used.

2. Model description

2.1. Equation of state

The most commonly used equation of state for a gas is the ideal gas equation. It links two important quantities, gas pressure p_{gas} and gas density ρ_{gas} .

$$p_{gas} = \rho_{gas} RT_{gas} = \frac{\rho_{gas}}{\psi_{gas}} \quad (1)$$

$$\rightarrow \rho_{gas} = \frac{p}{RT} = p \psi_{gas} \quad (2)$$

Here, R is the universal gas constant divided by the molar mass of the material (e.g. for air $R = (8.314472 \text{ [J/(mol K)]}) / (0.0289644 \text{ [kg/mol]}) \cong 287 \text{ [m}^2\text{/(s}^2 \text{ K})]$) and ψ_{gas} is the temperature dependent proportionality coefficient of density and pressure.

The liquid equation of state is described by a linear function in pressure [23-26].

$$\rho_{liquid} = p\psi_{liquid} + \rho_0 \quad (3)$$

Here the coefficient ψ_{liquid} is also indirectly proportional to the temperature (for the investigated interval of liquid temperature)

$$\psi_{gas} = \frac{b}{\tilde{R}_{liquid}T} \quad (4)$$

where $\tilde{R}_{liquid} = R/m_{mol,liquid}$ ($m_{mol,liquid}$ - molar mass of the liquid) and b , ρ_0 are material specific constants.

2.2. Governing equations

The following equations were implemented as a solver into the OpenFOAM[®] library in order to correctly simulate compressible and turbulent multiphase flows [27,41]. The continuity, the momentum and the energy equations are solved consecutively without a velocity pressure coupling. Multiple phases are implemented using the *volume-of-fluid method* where a scalar quantity α is used for the liquid phase volume fraction, that is transported with the velocity \mathbf{u} [28-29].

To the usual transport equation (color equation) of α an additional third term is added.

$$\frac{\partial \alpha}{\partial t} + \nabla \cdot (\mathbf{u}\alpha) + \nabla \cdot (\mathbf{u}_r \alpha (1 - \alpha)) = 0 \quad (5)$$

This surface compression with the compression velocity \mathbf{u}_r term helps maintaining a sharp liquid-gas interface. Further detail on this approach can be found in [27,30-32].

A mean density is calculated using the phase fraction which is then used in the following equations.

$$\rho = \alpha \rho_{liquid} + (1 - \alpha) \rho_{gas} \quad (6)$$

The continuity equation is solved with a variable density ρ .

$$\frac{\partial \rho}{\partial t} + \nabla \cdot (\rho \mathbf{u}) = 0 \quad (7)$$

The density is used for the calculation of the momentum equation. The value of the pressure p is calculated from the density ρ with the equation of state (see equations 2 and 3). The momentum equation is used in the form

$$\frac{\partial \rho \mathbf{u}}{\partial t} + \nabla \cdot (\rho \mathbf{u} \mathbf{u}) = -\nabla p + \nabla \cdot \rho \nu [\nabla \mathbf{u} + (\nabla \mathbf{u})^T] + \nabla \cdot \mathbf{B} + \mathbf{F}_\sigma \quad (8)$$

Here, ν is the laminar viscosity, the term \mathbf{F}_σ is the volumetric force density resulting from surface tension [31,33-34] and \mathbf{B} is the subgrid-scale stress tensor. Turbulence can be handled in many ways. The main approach used here is the '*DeardorffDiffStress*' LES turbulence model provided by OpenFOAM[®] [31]. It is a fully three-dimensional model [20,35] and such differential stress models (DSM) use a modeled version of the balance equation for \mathbf{B} .

In the next step the energy equation is solved

$$\frac{\partial E}{\partial t} + \nabla \cdot ((E + p)\mathbf{u}) = \nabla \cdot (\mathbf{h} + \mathbf{b}) \quad (9)$$

One has to consider the fact, that $E = \rho c_v T + 1/2 \rho \mathbf{u}^2$ is the sum of the specific internal and specific kinetic energy per unit mass with c_v being the specific heat at constant volume and T being the absolute temperature of the fluid. \mathbf{h} is the according vector of heat flux and \mathbf{b} is the subgrid-scale flux vector [35].

With the calculated value for T one can readjust the values for ψ_{gas} , ψ_l , ρ_{gas} and ρ_l in equations 1-4. Then a new time step is initiated and the procedure is repeated for each time step.

3. Single phase supersonic turbulent flow

To ensure the correct simulation of the supersonic part of the gaseous phase in later investigations a study of a single phase benchmark case is shown. In the multiphase solver the liquid phase fraction was set to zero in the whole domain and the thermophysical properties of air were used for the fluid [26].

3.1. Equation of state

A schematic sketch of the investigated geometry can be seen in figure 1, where the wall is indicated by the solid line. It consists of a 25° expansion and a 25° compression corner. The expansion and the compression of an incoming Mach 2.88 adiabatic turbulent boundary layer with the thickness of δ will be analyzed (for comparison see [16,18]). Figure 1 shows a schematic sketch of a slice through the domain. The expected shape of the expansion fan and the shock wave as well as the separation region are also shown in figure 1.

The geometric dimensions of the calculation domain are 24δ in the x-direction, 6δ in the y-direction and 2δ in the z-direction. Shown results are always evaluated on the $z = \delta$ plane to be comparable with [16,18] and the experimental data in [14-15]. 56 cells were used along the z-axis and an overall of 24000 cells were used on the x-y-plane.

The Reynolds number Re_δ of the investigated flow is 20000 in order to guarantee comparability with simulation results in the literature [16,18,36].

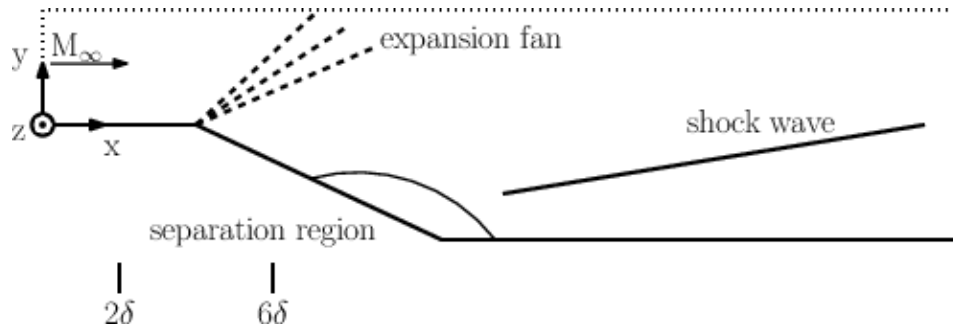


Figure 1. Schematic sketch of the investigated expansion-compression corner

3.2. Inlet conditions and boundary layer

For the correct simulation of the boundary layer on the inlet a separate simulation of an incoming flow over a flat plate ($M_\infty = 2.88$) was conducted. A computational domain with an x-dimension of 14.8δ , a y-dimension of 3.4δ and a z-dimension of 1.925δ (150x64x56 cells, as suggested in [36]) was used. The calculation was carried out over a time period of $320\delta/U_\infty$ and time averaged. This way a boundary layer δ with a thickness of $312.2 \mu\text{m}$ was found which is in good agreement with the value of $314.6 \mu\text{m}$ found in [36]. This boundary layer was used as the inlet condition for the expansion-compression corner.

3.3. Results

Simulation results were collected over the same simulated time period as in the simulation of the flat plate. Mean values during this period were calculated and used for evaluation. Figure

2 shows the mean pressure distribution in the calculation domain. One can clearly identify the expansion fan around the expansion corner as well as the pressure jump after the compression corner.

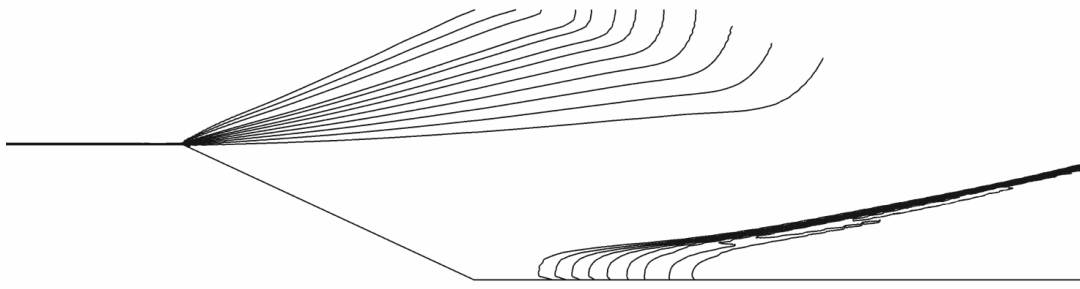


Figure 2. Iso-lines of mean pressure

A separation zone can be clearly identified around the second corner with the length L_{sep} (see figure 3). Both the pressure and the velocity distribution are in good agreement with results in [16,18] which themselves also resemble experimentally found results in [14-15].

In [16,18,37-38] a scaled separation length L_{sep}/L_c was introduced for experimental data with

$$L_c = \frac{\delta_e \left(\frac{p_2}{p_{pl}}\right)^{3.1}}{M_c^3} \quad (10)$$

Here, p_2 is the the pressure after the shock, p_{pl} is the plateau pressure from the formula of Zukoski [16,18,37-39] ($p_{pl} = p_c (2 M_c + 1)$), and M_c , p_c and δ_c are the Mach number, pressure value and the boundary layer thickness upstream of the compression and downstream of the expansion corner. In [16] this scaled value is given by 11.3 ± 1.2 (the error interval is given due to the uncertainty in the determination of δ_c). In this investigation the value was calculated to be 14.1 ± 1.4 . In [16] a comparison with experimental results was done by linear extrapolation from experimental results with higher Reynolds-numbers and good agreement is reported. If one assumes a non-linear behavior of the dependency on the Reynolds number the higher value of 14.1 can still be stated to be comparable to experimental results.

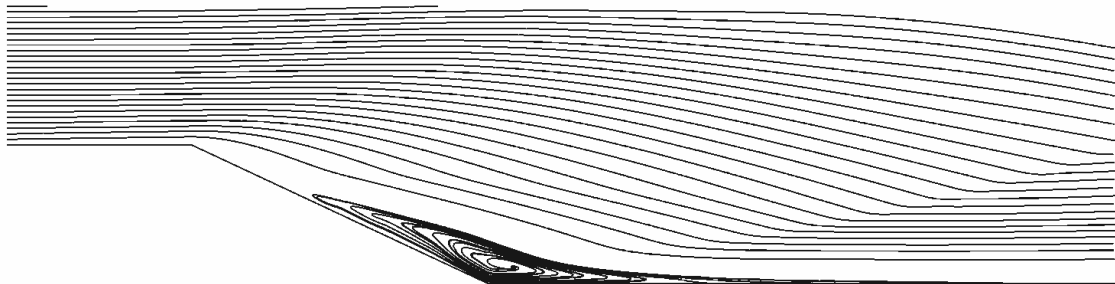


Figure 3. Mean streamlines showing the separation region

The surface pressure profile in figure 4 shows a drop in pressure after the first corner; where the value of the drop is correctly predicted by the simulation. The separation of the boundary layer around the second corner causes a plateau before the pressure value rises more abruptly again after the second corner. After the minimum the simulation results are above the experimental values. However, this is comparable to the experiments, as data show, that the pressure values on the plateau would be higher at lower Reynolds numbers (like for the used value of 20000 in the simulation).

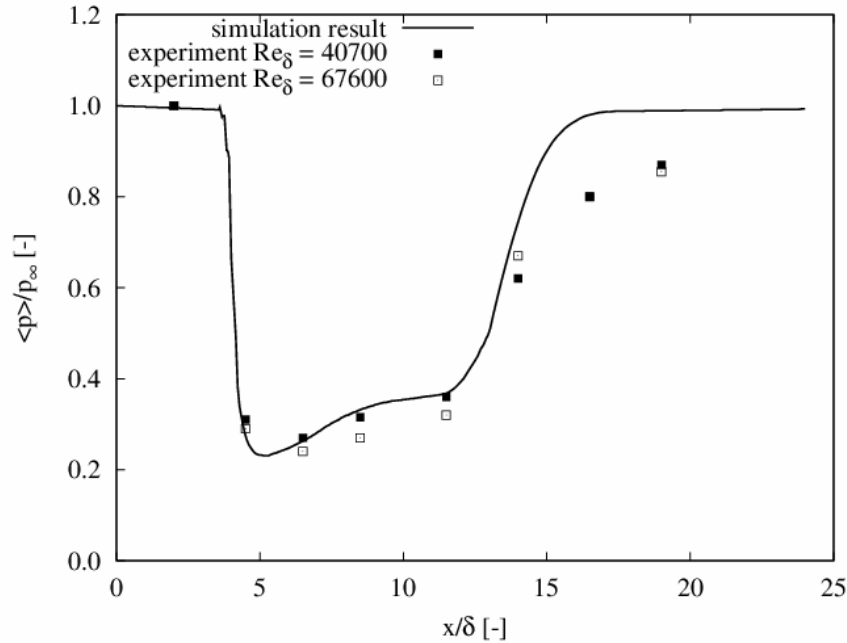


Figure 4. Mean pressure on solid surface (scaled)

Scaled velocity values at two lines located at $x = 2\delta$ and 6δ can be seen in figure 5. The first line is upstream of the expansion corner and the other line is between the corners (see figure 1). Results are in good consensus to the experimental values from [14].

An important issue here is the correct handling of turbulence. For that reason the scaled values of the first component of the stress tensor along the same lines as above are shown in figure 6. Upstream of the expansion fan turbulent effects are restricted to the boundary layer. However, after the corner turbulence is distributed over a wider area. A comparison with [16] shows a good agreement in the modeling of turbulence.

Concluding from the comparison of the simulation results one can say, that the used solver is able to predict expansion and compression phenomena in a high Mach number flow and also delivers a pressure and velocity distribution comparable to experimental and simulation results published in the literature.

4. Turbulent simulation of the aerobreakup of a liquid droplet

4.1. Introduction

In this section a simulation of a three-dimensional flow of a planar shock wave ($M = 3$) hitting a spherical water droplet with a diameter of 3.5 mm is shown (see figure 7). The location of the shock front at $t = 0 \mu\text{s}$ is 2 mm in the negative x -direction from the center of the droplet. Initial conditions in the positive x -direction of the shock front are

$$p = 0.1 \text{ MPa}, u_i = v_i = w_i = 0 \text{ m/s}, T_i = 346.98 \text{ K}$$

and in the negative x -direction

$$p = 1.0333 \text{ MPa}, u_i = 831.48 \text{ m/s}, v_i = w_i = 0 \text{ m/s}, T_i = 929.57 \text{ K}$$

These conditions are taken from [8] and applied to the three-dimensional case. The simulated region reaches from -0.012 m to 0.012 m in the x -direction and from -0.004 m to 0.004 m in the y - and z -direction.¹ Three different structured grids with 240x80x80,

¹ Simulations in larger regions were conducted, however no significant changes in the results were observed.

320x106x106 and 480x160x160 cells were investigated, providing a cell edge refinement of a factor of two in each Cartesian direction to ensure grid independent results.

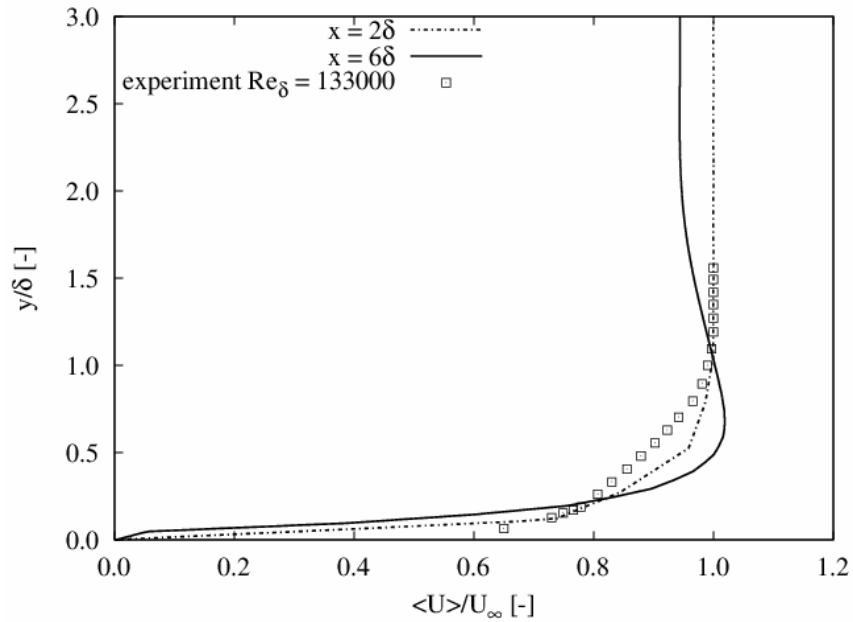


Figure 5. Mean velocity magnitude (scaled)

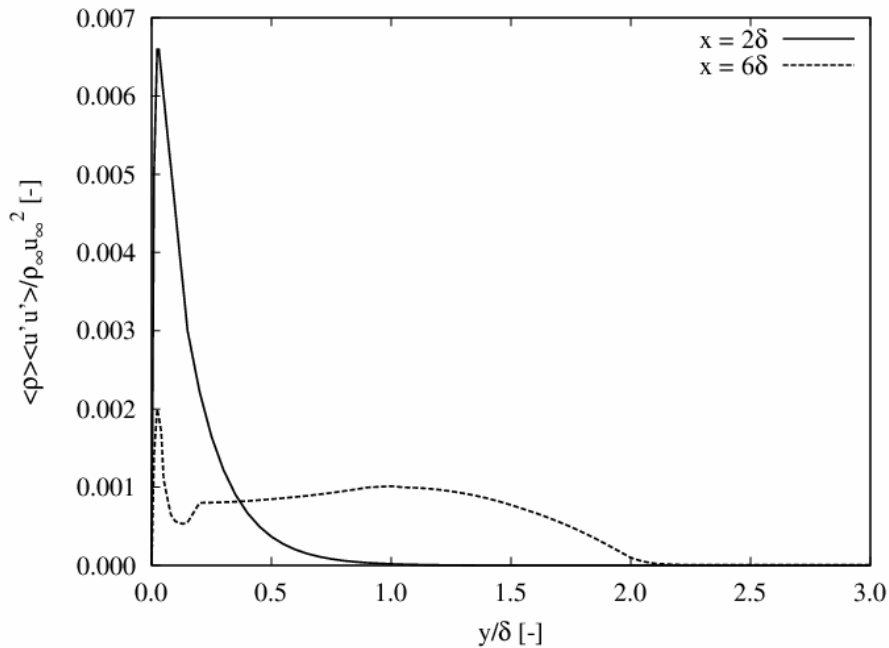


Figure 6. First component of the stress tensor (scaled)

As the computational domain does not include walls all the boundary conditions are set to 'zeroGradient' [31] (von Neumann type with the gradient set to zero). This boundary condition was found to produce no boundary artifacts such as pressure reflections in the given time interval. For the discretization of all the operators second order schemes have been utilized.

For the gaseous phase thermophysical data of air and for the liquid phase data of water were used [26]. The surface tension of water/air was set to a constant value of 0.07275 N/m. The

Weber number [6] for the calculated case is $We = \frac{\rho_{gas} u^2 d}{\sigma} = 128803$. Here, ρ_{gas} is the gas

density, u is the free-stream velocity, d is the droplet diameter and σ is the value of surface tension. The Ohnesorge number is $Oh = \frac{\mu_{liquid}}{\sqrt{\rho_{liquid}d\sigma}} = 0.002$ (this relates viscous to inertial and surface tension forces). Here, μ_{liquid} is the dynamic viscosity of the liquid and ρ_{liquid} is the liquid density. The Reynolds number is $Re = \frac{\rho_{gas}ud}{\mu_{gas}} = 194012$ (ratio of inertial forces to viscous forces), with μ_{gas} the gas dynamic viscosity. A certain time scale [6,40] is defined for this flow by $T^* = tud^{-1} \sqrt{\frac{\rho_{gas}}{\rho_{liquid}}}$. This way a characteristic dimensionless time $T = t/T^*$ can be given for the simulation with $T^* = 68.2 \mu s$. The simulation was carried out until $26 \mu s$ ($T = 0.38$). For reasons of numerical stability of the calculation a maximum CFL (Courant) number of 0.02 was used.

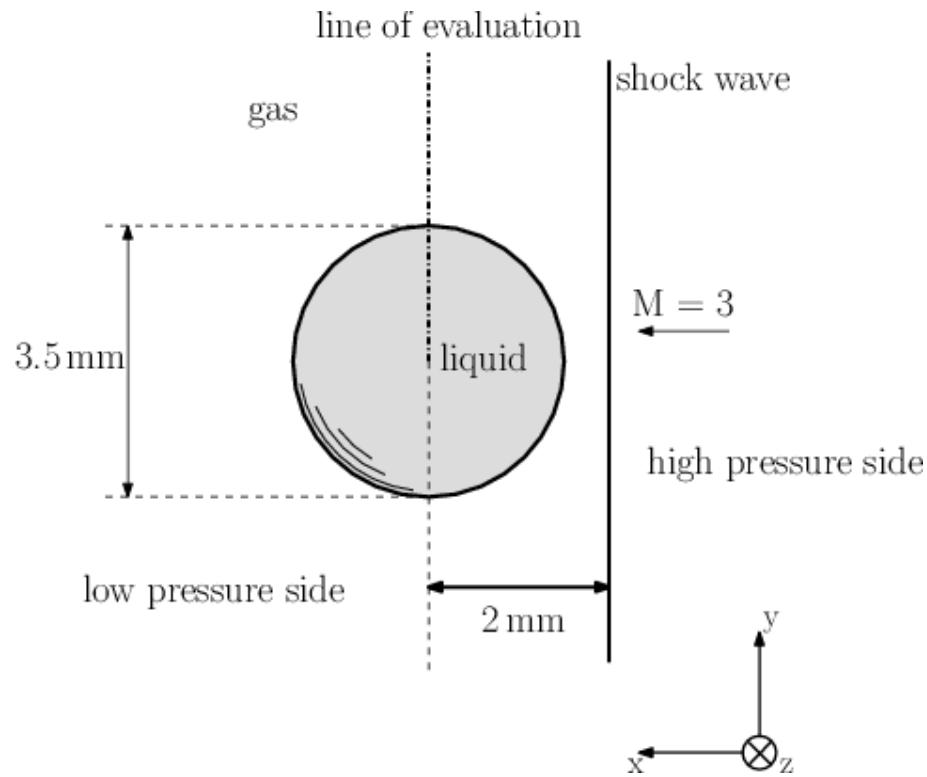


Figure 7. Schematic sketch of initial conditions (with the dash-dotted line of evaluation)

The experimental analysis of droplet breakup in different flows is limited to shadowgraph pictures [1,4,5,40] and visual interpretations. The images are limited by the resolution of the camera and the restricted information delivered by the two-dimensional outline of the droplet. Recently the laser-induced fluorescence method was able to deliver high resolution images of the surface of a liquid droplet during the process of breakup. This enables the three-dimensional interpretation of the process. For that reason the best experimental comparison with the results are found in [1]. The investigated phenomenon of shear-induced entrainment as the cause of droplet breakup occurs at $We > 1000$ [1]². Breakup processes with a higher Weber number are useful for comparisons.

² In [1] for the liquid phase mostly tributylphosphate (TBP) was used, however the droplet breakup of water is comparable if the Weber number is similar.

4.2. Discussion of results

For the visual comparison between simulation results and experiments [1] the deformation of the droplet after $T = 0.38$ is shown in figure 8 (surface of constant phase fraction value $\alpha = 0.9$, representing the surface of the droplet). The droplet is dissected by an evaluation plane colored by the velocity magnitude and overlaid with unscaled velocity vectors. One can see a stagnation zone in the gaseous phase in front of the droplet. In this region the droplet has a mirror smooth surface which is also reported in [1]. In this simulation the lateral extent of this area can be considered to be approximately 50 % of the initial droplet diameter.

At very early stages the velocity magnitude drops to the value of zero on the stagnant droplet. However, with increasing time shear and turbulent stress phenomena accelerate the surface region of the droplet, but the velocity still drops close to the surface. After the periphery of the 'smooth' region mentioned above the surface of the droplet becomes wavy and an outwardly directed flow drives the drop mass redistribution.

The most significant finding here is the stagnation zone in front of the droplet and its impact onto turbulence (on this also see [1]). The applied turbulence model shows relatively low values of the components of the subgrid-scale stress tensor for this region (see figure 9). Exactly at the periphery of this region, the magnitude of the subgrid-scale components rapidly increases resulting in a rapid transition from a laminar to a turbulent flow. Precisely at the location of high subgrid-scale turbulence values the wavy shape of the droplet surface emerges. This suggests a substantial effect of turbulence besides the macroscopic shear stress for high Weber number flows in simulations.

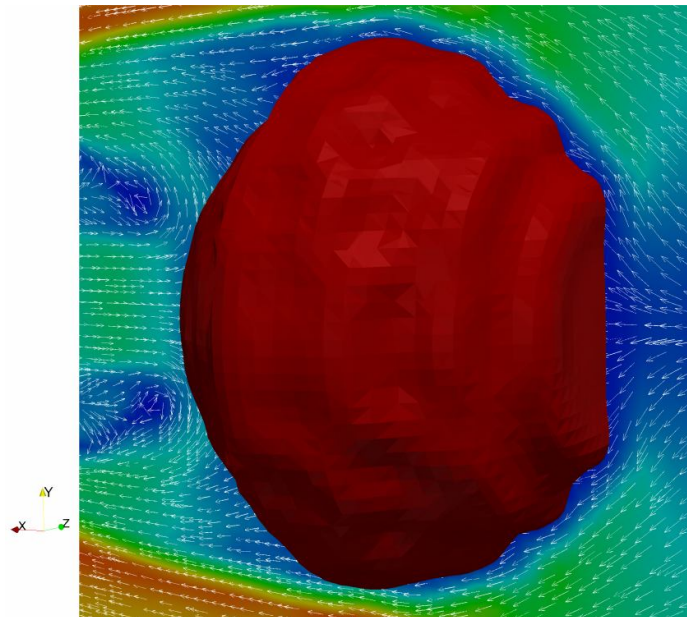


Figure 8. Contour plot of velocity magnitude with the surface of constant value of $\alpha = 0.9$ and the velocity vectors with constant length (at $T = 0.38$, values of velocity magnitude between 0 m/s (blue) and 1200 m/s (red))

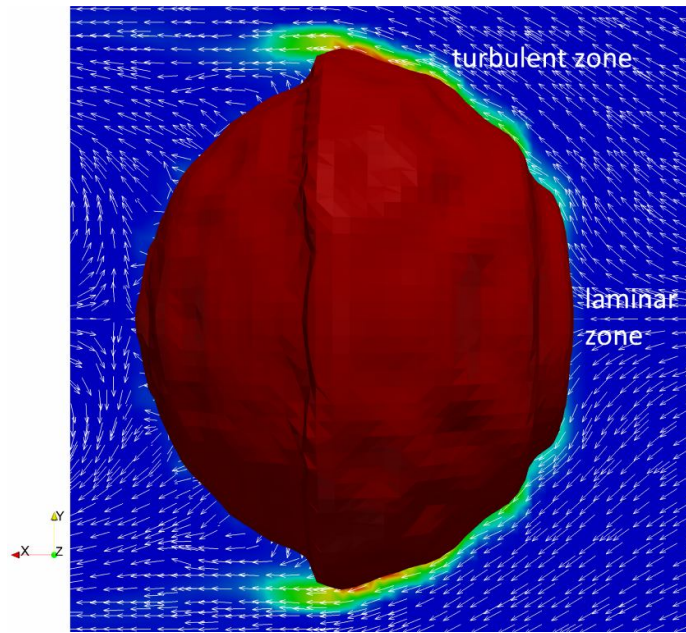


Figure 9. Contour plot of the first component of the subgrid-scale stress tensor $\rho u'u'$ with the surface of constant value of $\alpha = 0.9$ and the velocity vectors with constant length (at $T = 0.38$, red maximum, blue minimum)

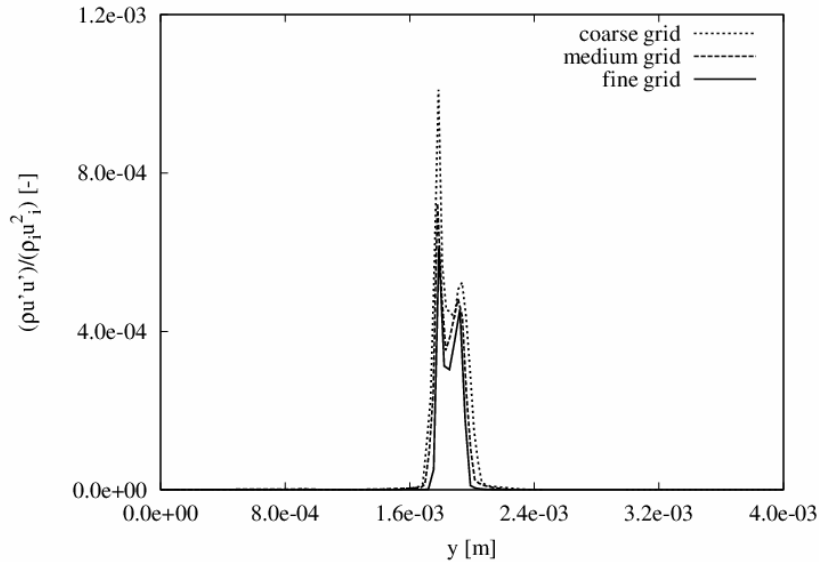


Figure 10. $\rho u'u'/\rho_i u_i^2$ at $T = 0.175$ on the evaluation line

To underline the theory presented above the grid convergence of the results at $T = 0.175$ is shown in figure 10. The value of the first subgrid-scale component $\rho u'u'$ scaled with the initial density and velocity is shown on the line (see figure 7) from the center of the original droplet at $x = y = z = 0$ m to $x = z = 0$ m and $y = 0.004$ m. It is noted, that for the initial density the value of $\rho_i = \alpha \rho_{li} + (1 - \alpha) \rho_{gi}$ is used. The value of $\alpha = 0.5$ is approximately at $y = 0.0019$ m. The results on all three grids are converging with the refinement of the grid. In figure 10 two maxima can be seen which occur in the simulation due to a different increase in $u'u'$ and decrease in ρ at the surface of the droplet.

If all the six components of the symmetric subgrid-scale tensor are compared, one can clearly identify the dominating factors in this case. The diagonal elements of the tensor are of highest magnitude (see figure 11), however the component $\rho u'v'$ is just one order of magnitude

smaller (see figure 12). The components $\rho v'v'$ and $\rho w'w'$ are practically equal due to the equal distribution of turbulence amongst these components which is a sign for the radial transport of turbulence on the surface downstream of the frontal region (for comparison of the radial component of the flow in the experiments see [1]). The other two off-diagonal components (see figure 12) appear to be five orders of magnitude lower than the diagonal elements thus being practically negligible.

In [1] the authors state, that instead of the Rayleigh–Taylor piercing, the dominant mechanism is the shear-induced entrainment with a significant radial component and instabilities on the so-generated liquid sheet. In figure 13 the value of $(\rho u'u')/(\mu \partial_x u)$ is shown, with $\mu = \alpha \mu_i + (1 - \alpha) \mu_l$ being the weighted dynamic viscosity of the gaseous and the liquid phase. Computational results in this work support the theory in [1] and additionally show, that in simulations with a given cell size subgrid-scale turbulent effects are even one to two orders of magnitude higher than shear phenomena.

This shows, that subgrid-scale turbulence effects cannot be neglected in simulations. Thus for the correct simulation of the initial stages of the breakup of liquid droplets one either has to ensure the resolution of the Kolmogorov scales (in the case of DNS) or in case the required resolutions are computationally unreachable, one has to model turbulence with a suitable model. Also three-dimensionality has to be guaranteed for the correct handling of turbulence.

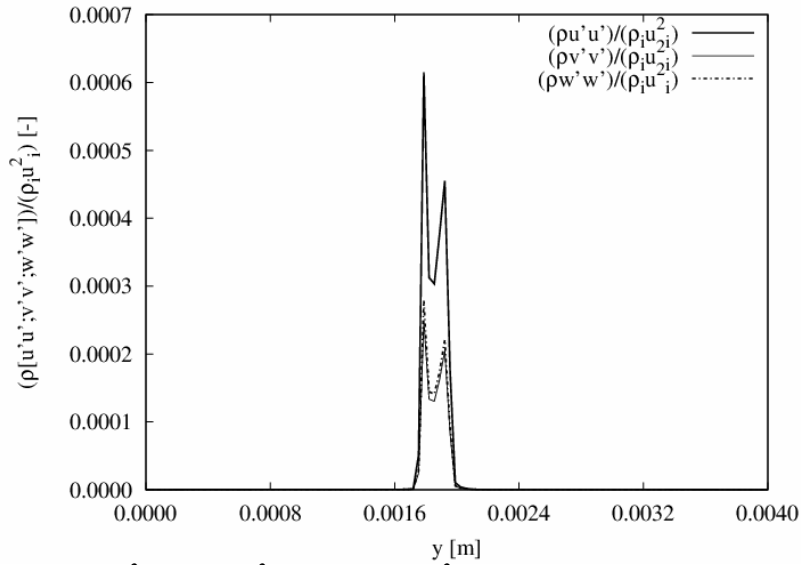


Figure 11. $\rho u'u'/\rho_i u_i^2$, $\rho v'v'/\rho_i u_i^2$ and $\rho w'w'/\rho_i u_i^2$ at $T = 0.175$ on the line of evaluation

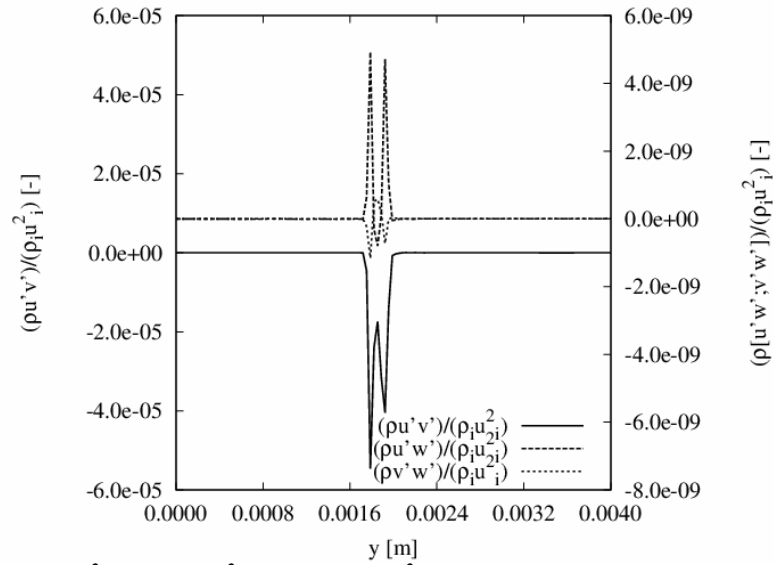


Figure 12. $\rho u'v'/\rho_1 u_1^2$, $\rho u'w'/\rho_1 u_1^2$ and $\rho v'w'/\rho_1 u_1^2$ at $T = 0.175$ on the line of evaluation

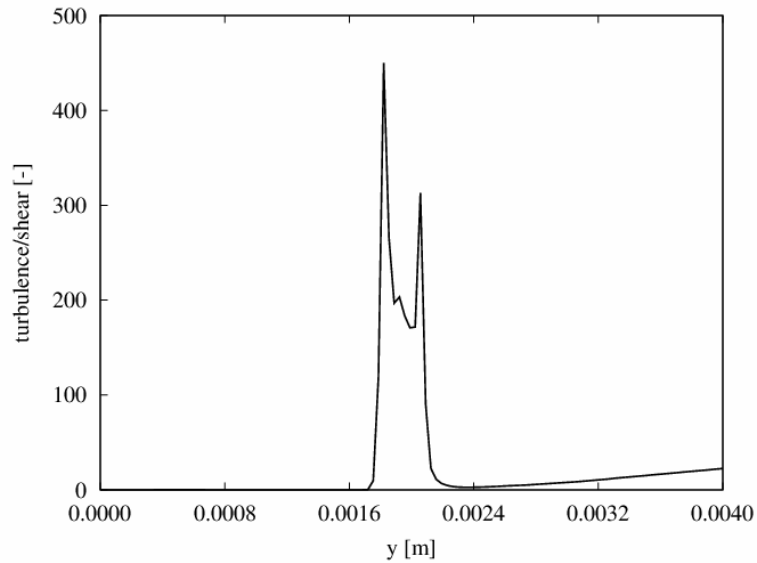


Figure 13. Comparison of turbulence and shear stress phenomena at $T = 0.175$ on the line of evaluation

The physical interpretation of the simulation results suggest, that turbulence phenomena are one of the dominant factors during the breakup of droplets in a high Weber number flow resulting in the characteristic shape of the redistributed liquid mass on the surface of the droplet. One can clearly identify a laminar and a turbulent zone on the front side of the droplet as well as a rapid transition between these two regions resulting in the characteristic shape of the droplet during the initial stages of the breakup process.

Further discussion on the quality of the LES results with special focus on different turbulence models can be found in [41].

5. Conclusion

In this work simulation results of a high Weber number multiphase flow with turbulence modeling of the initial stages of the breakup of a droplet are shown. As a first step the correct

handling of turbulence in a Mach 2.88 single phase flow was ensured by comparison with other simulation and experimental results.

The turbulent simulation of the droplet breakup shows the importance of the subgrid-scale turbulence modeling. One can clearly identify a stagnant low velocity zone in front of the droplet and a high velocity zone around the droplet. On the threshold between these two zones turbulence effects emerge resulting in the characteristic shape of the droplet during the breakup process at Weber numbers higher than 1000.

Nomenclature

Roman

b	material constant for liquid equation of state
\mathbf{b}	subgrid-scale heat flux vector
\mathbf{B}	subgrid-scale stress tensor
c_v	specific heat
d	diameter
E	energy
\mathbf{F}	volumetric force density
\mathbf{h}	heat flux vector
L	length
M	Mach number
p	pressure
R	universal gas constant
t	time
T	temperature
\mathbf{u}	velocity vector
u, v, w	Cartesian velocity components

Greek

α	liquid phase fraction
δ	boundary layer thickness
μ	dynamic viscosity
ν	kinematic viscosity
ρ	density
σ	surface tension
ψ	temperature dependent proportionality coefficient in equation of state

Indices

0	constant
2	after shock
c	upstream of compression and downstream of expansion corner
gas	gaseous
i	initial
$liquid$	liquid
pl	plateau
r	compression
sep	separation
σ	surface tension

Superscripts:

'	subgrid-scale
---	---------------

References

- [1] T.G. Theofanus and G.J. Li. *On the physics of aerobreakup*. Phys Fluids, 20:052103–01–052103–14, 2008.
- [2] H. Zhao, H.-F. Liu, X.-K. Cao, W.-F. Li, and J.-L. Xu. *Breakup characteristics of liquid drops in bag regime by a continuous and uniform air jet flow*. Int J.Multiphase Flow, 2011.

- [3] Ch.-L. Ng and T.G. Theofanous. *Modes of aero-breakup with visco-elastic liquids*. in *Proceedings of XVth International Congress on Rheology*, California, USA, August 2008.
- [4] D.D. Joseph, J. Belanger, and G.S. Beavers. *Breakup of a liquid drop suddenly exposed to a high-speed airstream*. *Int J. Multiphase Flow* **25**, 1999, p.1263–1303.
- [5] T. Theofanous, G. Li, and T. Dinh. *Aerobreakup in rarefied supersonic gas flows*. *J. Fluids Eng.* **126**, 2004, p.516–527.
- [6] T.G. Theofanous, G.J. Li, T.N. Dinh, and C.-H. Chang. *Aerobreakup in disturbed subsonic and supersonic flow field*. *J. Fluid Mech.* **593**, 2007, p.131–170.
- [7] R.R. Nourgaliev, T.N. Dinh, and T.G. Theofanous. *Adaptive characteristics-based matching for compressible multifluid dynamics*. *J. Comput. Phys.* **213**, 2006, p. 500–529.
- [8] C.-H. Chang and M.-S. Liou. *A robust and accurate approach to computing compressible multiphase flow: Stratified flow model and AUSM⁺-up scheme*. *J. Comput. Phys.* **225**, 2007, p. 840–873.
- [9] H. Terashima and G. Tryggvason. *A front-tracking/ghost-fluid method for fluid interfaces in compressible flows*. *J. Comput. Phys.* **228**, 2009, 4012–4037.
- [10] H. Terashima and G. Tryggvason. *A front-tracking method with projected interface conditions for compressible multi-fluid flows*. *Computers & Fluids* **39**, 2010, p. 1804–1814.
- [11] R.R. Nourgaliev, S.Y. Sushchikh, T.N. Dinh, and T.G. Theofanous. *Shock wave refraction patterns at interfaces*. *J. Multiphase Flow* **31**, 2005, p. 969–995.
- [12] M.-S. Liou, C.-H. Chang, H. Chen, and J.-J. Hu. *Numerical study of shock-driven deformation of interfaces*. *Shock Waves* **XII**, 2009, p. 919–924.
- [13] T. Theofanous, R. Nourgaliev, G. Li, and N. Dinh. *Compressible multi-hydrodynamics (cmh): Breakup, mixing, and dispersal, of liquids/solids in high speed flows*. in *Proceedings of the YUTAM Symposium on Computational Approaches to Disperse Multiphase Flow*, 2006, p. 353–369, Dordrecht, Netherlands.
- [14] A. Zheltovodov, V. Trofimov, E. Filippova, and Y. Takovlev. *Influence of turbulence change on the heat exchange under the conditions of supersonic separated flows*. in *Proceedings of the YUTAM Symposium on Separated Flows and Jets*, 1990, p. 273–274, USSR Academy of Sciences, Siberian Division, Novosibirsk.
- [15] A. Zheltovodov, V. Trofimov, E. Schuelein, and T. Yakovlev. *An experimental documentation of supersonic turbulent flows in the vicinity of forward- and backward-facing ramps*, 1990. ITAM Report.
- [16] D. Knight, H. Yan, , and A. Zheltovodov. *Large eddy simulation of supersonic turbulent flow in expansion-compression corner*. in *Proceedings of the Third AFOSR International Conference on DNS/LES*, 2001, Arlington, Texas, USA.
- [17] H. Yan, D. Kight, and A. A. Zheltovodov. *Large eddy simulation of supersonic compression corner using eno scheme*. in *Proceedings of the Third AFOSR International Conference on DNS/LES*, 2001, Arlington, Texas, USA.
- [18] D. Knight, H. Yan, A. G. Panaras, and A. Zheltovodov. *Advances in CFD prediction of shock wave turbulent boundary layer interactions*, 2006. NATO Report.
- [19] J.P. Dussauge, R.W. Smith, A.J. Smits, H. Fernholz, P.J. Finley, and E.F. Spina. *Turbulent Boundary Layers in Subsonic and Supersonic Flow*. Advisory Group for Aerospace Research and Development, 1996.
- [20] H. Weller, G. Tabor, H. Jasak, and C. Fureby. *A tensorial approach to continuum mechanics using object-oriented techniques*. *J. Comput. Phys.* **12**(6), 1998, p. 620–631.
- [21] H. Jasak, H. Weller, and N. Nordin. *In-cylinder CFD simulation using a C++ object-oriented toolkit*. SAE Paper 2004-01-0110, 2004.

- [22] H. Jasak. *Error analysis and estimation for the finite volume method with applications to fluid flows*, Ph.D. thesis. UK: Imperial College of Science, Technology and Medicine., 1996.
- [23] R. Menikoff and B. J. Plohr. *The Riemann problem for fluid flow of real materials*. Rev. Mod. Phys. **61**(1), 1989, p. 75–130.
- [24] R. Saurel and R. Abgrall. *A simple method for compressible multifluid flows*. SIAM J. Sci. Comput. **21**(1), 1999, p. 1115–1145.
- [25] J.-P. Cocchi and R. Saurel. *A Riemann problem based method for the resolution of compressible multimaterial flows*. J. Comput. Phys. **137**, 1997, p. 265–298.
- [26] U.S. Secretary of Commerce. *NIST Chemistry WebBook*, 2011. <http://webbook.nist.gov/>.
- [27] J. Nagy, C. Jordan, and M. Harasek. *Technical application of a multiphase solver in the compressible flow of a gaseous and a liquid phase*. in *Proceedings of the 8th International Conference on CFD in Oil and Gas, Metallurgical and Process Industries*, Trondheim, Norway, 2011.
- [28] A. Pecenko, L.G.M. van Deurzen, J.G.M. Kuerten, and C.W.M. van der Geld. *Non-isothermal two-phase flow with a diffuse-interface model*. Int. J. Multiphase Flow **37**, 2011, p. 149–165.
- [29] H. Rusche. *Computational Fluid Dynamics of Dispersed Two-Phase Flows at High Phase Fractions*. Ph.D. thesis. Imperial College of Science, Technology & Medicine, Department of Mechanical Engineering, 2002.
- [30] CGI/OpenFOAM Foundation. *OpenFOAM[®] User Guide*. OpenCFD Limited, 10th edition, 2009.
- [31] CGI/OpenFOAM Foundation. *OpenFOAM[®] source code*, 2011. <http://www.openfoam.com/>.
- [32] M. Raessi, J. Mostaghimi, and M. Bussmann. *A volume-of-fluid interfacial flow solver with advected normals*. Computers & Fluids **39**, 2010, p. 1401–1410, 2010.
- [33] W. Dijkhuizen, M. van Sint Annaland, and H. Kuipers. *Numerical investigation of closures for interface forces in dispersed flows using a 3D front tracking model*. In *Fourth International Conference on CFD in the Oil and Gas, Metallurgical and Process Industries*. SINTEF/NTNU Trondheim, Norway, 2005.
- [34] J.U. Brackbill, D.B. Kothe, and C. Zemach. *A continuum method for modeling surface tension*. J. Comput. Phys. **100**, 1992, p. 335–354.
- [35] C. Fureby and F. F. Grinstein. *Large eddy simulation of high-reynolds-number free and wall-bounded flows*. Journal of Computational Physics **181**, 2002, p. 68–97.
- [36] C. Kannepalli, S. Arunajatesan, and S.M. Dash. *RANS/LES methodology for supersonic transverse jet interactions with approach flow*. AIAA paper, 2002.
- [37] A. Zheltovodov and E. Schuelein. *Peculiarities of turbulent separation development in disturbed boundary layers*. Modelirovaniye v Mekhanike **2**(1), 1988, p. 53–58.
- [38] A. Zheltovodov, E. Schuelein, and C. Horstmann. *Development of separation in the region of interaction of shock wave with turbulent boundary layer disturbed by expansion*. Journal of Applied Mechanics and Technical Physics **3**, 1993, p. 58–68.
- [39] E. Zukoski. *Turbulent boundary layer separation in front of a forward facing step*. AIAA Journal **5**(10), 1967, p. 1746–1753.
- [40] O. G. Engel. *Fragmentation of water drops in the zone behind an air shock*. J. Res. Natl Bur. **60**, 1958, 245–280.
- [41] J. Nagy and M. Harasek. *Investigation of the aerobreakup of a liquid droplet at high Weber number with different turbulence models*. in *Proceedings of the 5th International Conference from Scientific Computing to Computational Engineering*, Athens, Greece, July 2012.